Clays and Clay Minerals, Vol. 64, No. 4, 438–451, 2016.

COMPARATIVE COMPUTATIONAL STUDY OF Np(V) AND U(VI) ADSORPTION ON (110) EDGE SURFACES OF MONTMORILLONITE

ALENA KREMLEVA* AND SVEN KRÜGER

Department Chemie, Technische Universität München, 85747 Garching, Germany

Abstract—Sorption of U(VI) on clay and related minerals has been inspected experimentally and computationally because of its central role in safety considerations of geological repositories for highly radioactive waste. Np(V), which also has long half-life isotopes, has received considerably less attention. The purpose of the present study was to investigate computationally the adsorption of Np(V) on a clay-mineral surface and to compare it to adsorption of U(VI). As a sample case study, adsorption of Np(V) at the (110) edge surface of the common clay mineral montmorillonite was modeled. The density functional approach and periodic supercell models were applied. Mono- and bidentate adsorption complexes with coordination numbers 4 and 5 were inspected and compared to corresponding U(VI) species. While U(VI) prefers bidentate adsorption complexes with varying coordination numbers, Np(V) is more stable when monodentate-coordinated with a coordination number of four. In line with its smaller hydrolysis constant in aqueous solution, Np(V) shows a lower tendency to form monohydroxides on the mineral surface compared to U(VI). As no experimental geometry parameters are available for Np(V) adsorbed on montmorillonite, the results were compared tentatively to EXAFS data for adsorption at kaolinite and good agreement for the geometry changes due to adsorption was found for the more preferred adsorbed species.

Key Words—Actinide, Adsorption, Clay Minerals, Computational Modeling, Density Functional Theory, Edge Surface, Montmorillonite, Np(V), U(VI), Neptunyl, Uranyl.

INTRODUCTION

The interaction of radionuclides with mineral surfaces is of fundamental importance for understanding and the reliable prediction of the fate of these hazardous materials in the environment (Butler, 2010; Geckeis *et al.*, 2013). Risk assessment of a potential deep geological repository for radioactive waste is an area of particular concern because adsorption at mineral surfaces is regarded as an efficient retardation process (Butler, 2010; Geckeis *et al.*, 2013). A comprehensive description of the radionuclide interaction with solvated mineral surfaces at the molecular level should form the basis for thermodynamic modeling, which is a prerequisite for the assessment of the distribution of long-lived radionuclides in the geosphere (Bradbury and Baeyens, 2005a; Marques Fernandes *et al.*, 2012). With respect to adsorption, one of the most studied actinides to date has been U(VI), the main constituent of radioactive waste (Dent *et al.*, 1992; Chisholm-Brause *et al.*, 1994; Morris *et al.*, 1994; Sylwester *et al.*, 2000; Den Auwer *et al.*, 2003; Kowal-Fouchard *et al.*, 2004; Greathouse and Cygan, 2005, 2006; Schlegel and Descostes, 2009; Lectez *et al.*, 2012; Marques Fernandes *et al.*, 2012; Müller *et al.*, 2012; Geckeis *et al.*, 2013; Kremleva *et al.*, 2008, 2011, 2015, 2016). In the present work, the first computational study of the adsorption of Np(V) on a mineral surface is presented. Among other various radionuclides present in typical nuclear waste, Np is of particular interest. Due to the long half-life of Np^{237} (2.14×10^6 y), it will be a major contributor to radiotoxicity after a storage time of ~10^6 y (Bidoglio *et al.*, 1985). Compared to U(VI), knowledge of Np(V) sorption properties is limited. Some experiments have been done on adsorption on iron oxides (Arai *et al.*, 2007), kaolinite (Niitsu *et al.*, 1997; Reich *et al.*, 2007; Amayri *et al.*, 2008, 2011; Schmeide and Bernhard, 2010), gibbsite (Müller *et al.*, 2009; Gückel *et al.*, 2013), montmorillonite (Bradbury and Baeyens, 2005b; Turner *et al.*, 1998), silica (Del Nero *et al.*, 2004), and alumina (Del Nero *et al.*, 2004; Tochiyama *et al.*, 1996). The experimental methods include batch experiments (Tochiyama *et al.*, 1996; Niitsu *et al.*, 1997; Turner *et al.*, 1998; Del Nero *et al.*, 2004; Bradbury and Baeyens, 2005b; Arai *et al.*, 2007; Schmeide and Bernhard, 2010; Amayri *et al.*, 2011; Fröhlich, 2015), Fourier-transform infrared spectroscopy (FTIR) (Müller *et al.*, 2009; Gückel *et al.*, 2013), and extended X-ray absorption fine structure (EXAFS) (Arai *et al.*, 2007; Reich *et al.*, 2007; Amayri *et al.*, 2008; Gückel *et al.*, 2013).

In the present study, the adsorption of Np(V) on montmorillonite edge surfaces was investigated and compared to the adsorption of U(VI) (Kremleva *et al.*, 2015, 2016). Montmorillonite is the main constituent of

* E-mail address of corresponding author:
kremleva@mytum.de
DOI: 10.1346/CCMN.2016.0640408

This paper is published as part of a special issue on the subject of 'Computational Molecular Modeling.' Some of the papers were presented during the 2015 Clay Minerals Society-Euroclay Conference held in Edinburgh, UK.

bentonite, a commonly used barrier material. In aqueous solution, Np(V) exists as the neptunyl ion, NpO_2^+ (Cotton, 2006), which represents the most stable oxidation state under environmental conditions and shows a high solubility compared to other oxidation states (Cotton, 2006). Batch sorption experiments of Np(V) on montmorillonite have shown that in the pH range from 2 to 11 the sorption of Np(V) is typically weaker than that of U(VI) and it starts at a higher pH (Turner *et al.*, 1998). This infers that Np(V) forms weaker complexes with the surface compared to U(VI), in agreement with its lower charge. In the presence of carbonate in solution, Np(V) sorption peaked at pH 8−8.5 and decreased for more alkaline conditions (Turner *et al.*, 1998). A surface complexation model for Np(V) adsorption on montmorillonite was developed by Turner *et al.* (1998), assuming inner-sphere complexes on aluminol and silanol sites. The concept of strong and weak sites for Np(V) adsorption was introduced by Bradbury and Baeyens (2005b) who related the corresponding complexation constants with the hydrolysis constants of neptunyl. No information is available, however, about which sites on the surface correspond to strong and weak ones or whether adsorption of Np(V) differs from U(VI) at the atomic scale. The only experimental methods giving structural information about adsorption complexes are EXAFS and FTIR spectroscopy and, to the authors' knowledge, no EXAFS or FTIR data exist for Np(V) adsorbed on montmorillonite or any other structurally similar 2:1 aluminosilicate. An EXAFS study of Np(V) adsorption on gibbsite claimed inner-sphere bidentate adsorption because of the Np−Al distance resolved at ~330 Å, which is possible only for a bidentate surface complex (Gückel *et al.*, 2013). The EXAFS data for Np(V) adsorption on kaolinite (Reich *et al.*, 2007; Amayri *et al.*, 2008) do not include Np−Al/Si distances, nor do they show split Np−O distances in the first equatorial coordination shell of NpO_2^+. Nevertheless, these results were also interpreted as inner-sphere adsorption on edge surfaces (Amayri *et al.*, 2008). Inner-sphere adsorption was assumed also because of the relatively high pH in these experiments. For acidic conditions, where adsorption is considerably weaker, outer-sphere adsorption was postulated due to the ion-exchange mechanism (Zavarin *et al.*, 2012; Benedicto *et al.*, 2014). This aspect is beyond the scope of the present study, however, because the acidic pH is less relevant from an environmental perspective. A common expectation is that Np(V) adsorption on montmorillonite is similar to that of U(VI) (Turner *et al.*, 1998; Bradbury and Baeyens, 2005b). For this reason, the same models as for U(VI) adsorption are used to study Np(V) adsorption on montmorillonite (Kremleva *et al.*, 2015, 2016).

The purpose of the present study was to use computational methods to model the inner-sphere adsorption of Np(V) on the partially deprotonated exemplary (110) surface of montmorillonite. Using the recently introduced low-temperature simulated annealing procedure (Kremleva *et al.*, 2016) for pre-equilibration, relative energies of adsorption for complexes on various adsorption sites were calculated and the most stable ones determined. These were compared with the most stable adsorption complexes of U(VI) (Kremleva *et al.*, 2016).

METHODS AND MODELS

Computational method

First-principles density functional calculations were carried out on supercell slab models of the (110) edge surface of montmorillonite using the plane-wave based Vienna *ab initio* simulation package, *VASP* (Kresse and Hafner, 1993a, 1993b, 1994; Kresse and Fürthmuller, 1996a, 1996b). Electronic structure calculations were done by applying a GGA (generalized gradient approximation) exchange-correlation potential, PW91, as parameterized by Perdew and Wang (1992). Open-shell calculations were performed for all adsorption complexes of NpO_2^+. All of these converged to a triplet as the lowest-energy spin state. For the most stable complexes, singlet states were also optimized and found to be at least 50 kJ mol^{-1} less stable than the corresponding triplets. The effect of the core electrons was represented by the full-potential projector-augmented wave (PAW) method as implemented in *VASP* (Blöchl, 1994; Kresse and Joubert, 1999). Scalar relativistic effects were incorporated in the PAW potential *via* mass-velocity and Darwin corrections (MacDonald and Vosko, 1979). To estimate spin-orbit effects, a spin-orbit correction was calculated for exemplary structures in single-point fashion. In *VASP*, spin-orbit coupling is implemented with a relativistic Hamiltonian up to the order of α^2 (MacDonald *et al.*, 1980), including non-collinear magnetism (Tettenhorst and Roberson, 1973). The spin-orbit effect on total energies was calculated to be <4 kJ mol^{-1} for a set of five adsorption complexes, which does not affect any of the energy trends discussed below.

An energy cutoff of 400 eV was adopted for the surface models. Integrations over the Brillouin zone were carried out using the Γ-point only. In geometry optimizations the total energy was converged to 10^{-5} eV and forces acting on ions were required to be $<2 \times 10^{-4}$ eV/pm. In order to pre-equilibrate the structure of the water layer used to model surface solvation, a recently developed low-temperature simulated annealing procedure was applied (Kremleva *et al.*, 2016). Systems were equilibrated at 200 K for a few ps and then cooled to 0 K over the period of 1 ps. The temperature was adjusted to 200 K every 50 steps; the microcanonical ensemble, *NVE*, was used in between. The time step was adjusted to 0.2 fs and the energy cutoff was set to 300 eV. The pre-equilibrated systems were optimized subsequently with the more accurate parameters given

https://doi.org/10.1346/CCMN.2016.0640408 Published online by Cambridge University Press

above. In order to check if a system is equilibrated, a geometry optimization was done after each ps of equilibration; when the energies of two consecutive optimizations agreed within 10 kJ mol^{-1}, the system was assumed to have reached an approximately equilibrated state. Note that the final structures analyzed in the present study were obtained by geometry optimization. A full dynamical treatment of the systems studied was not undertaken to reduce the computational costs.

The program *VASP* provides accurate compensating corrections for charged unit cells of cubic lattices only (Lo and Trout, 2004). As in previous studies (Kremleva *et al.*, 2015, 2016) on uranyl adsorbed at edge surfaces of clay minerals, neutral unit cells were used, therefore. Restricting that study to sites with an overall charge of −2 *e*, two protons from the surface were removed to compensate the charge of adsorbed uranyl. In the present study, the models focused on Np(V) adsorbed at an edge surface with a doubly deprotonated unit cell. In order to neutralize the unit cell for adsorbed Np(V), a proton was attached to the bottom of the slab. The present results can thus be compared directly with those for uranyl studied previously (Kremleva *et al.*, 2015, 2016). For comparison, Np(V) and U(VI) aquo ions were equilibrated and optimized in a water box with 64 H_2O molecules. Data are provided here for the aquo neptunyl ion with coordination numbers (CN) 4 and 5 and for uranyl with CN = 5.

Surface and adsorption complex models

The 2:1 clay mineral montmorillonite is composed of an Al octahedral sheet that is sandwiched between two Si tetrahedral sheets. The layers contain negatively charged cation substitutions which are compensated by solvated counterions between the layers. Montmorillonite is the end-member of dioctahedral smectites with little or no tetrahedral substitution (Tettenhorst and Roberson, 1973) and its layer charge is mainly generated by substitution of Al^{3+} by Mg^{2+} in the octahedral sheet. A montmorillonite model with the stoichiometric formula $Na_{0.25}[Si_4(Al_{1.75}Mg_{0.25})O_{10}(OH)_2]$ with a layer charge of 0.25 *e* per formula unit was inspected.

The bulk and surface models used in the present study consisted of four formula units per unit cell with a single substitution (Kremleva *et al.*, 2016). The interlayer space contained eight water molecules in addition to one Na^+ per unit cell. The optimized bulk structure was used to create the (110) edge surface of montmorillonite with a 2×1 surface unit cell of ~10 Å × 13 Å surface area (Kremleva *et al.*, 2015, 2016). The substitution in the surface models was placed either in the second outermost cation layer from the surface, which is termed a subsurface substitution (Figure 1a) or directly on the surface and is then called a surface substitution (Figure 1b). When Mg occupies the subsurface position (Figure 1a), the surface is referred to as "unsubstituted" and the corresponding sites on it as "unsubstituted sites". If Mg is on the surface (Figure 1b), the surface is referred to as "substituted". The (110) edge surface with subsurface substitutions exhibits SiOH, $AlOH_2^{+1/2}$, and $AlO_mSi^{-1/2}$ groups, where a mixed center O_m connects Al and Si cations (Figure 1). Formal partial charges of surface O(H) groups, which are helpful in the interpretation of the results, were derived from Pauling's bond valence theory (Pauling, 1929). For further details

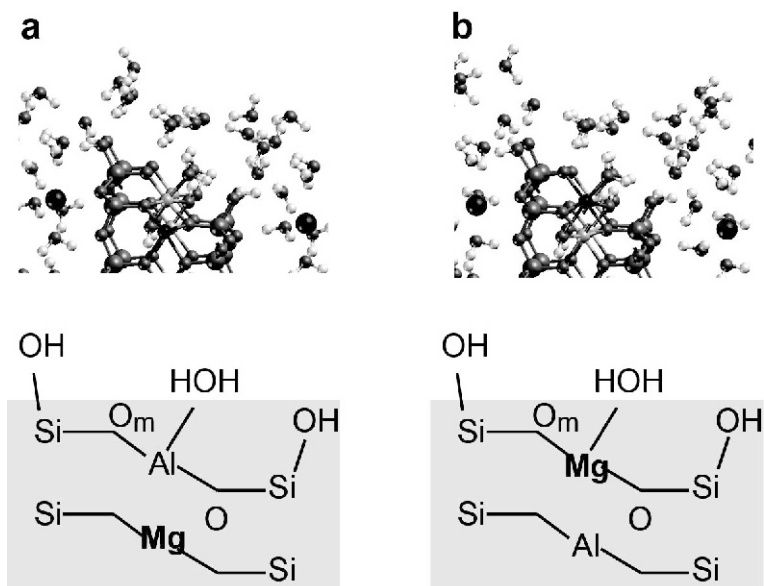

Figure 1. (a) Unsubstituted and (b) substituted (110) edge surfaces of montmorillonite.

https://doi.org/10.1346/CCMN.2016.0640408 Published online by Cambridge University Press

of bulk and surface models the reader is referred to Kremleva *et al.* (2015, 2016).

All models in the present study focused on complexes adsorbed on a doubly deprotonated surface unit cell. This surface model can be regarded as realistic because Np(V) adsorption starts at pH 7 (Turner *et al.*, 1998), where montmorillonite edge surfaces are partially deprotonated and negatively charged (Kosmulski, 2012). Four deprotonation schemes were taken into account (Figure 2). To estimate which deprotonation scheme is more likely, one may refer to the intrinsic pK_a values of various surface OH_2 and OH groups that were calculated recently using an accurate first-principles molecular dynamics approach, "FPMD" (Liu *et al.*, 2014). The $AlOH_2$ group was shown to be the most acidic with a pK_a value estimated at 5.5 while SiOH groups exhibited a pK_a of ~8 (Liu *et al.*, 2014). Thus, $AlOH_2$ and SiOH groups deprotonate first with increasing pH, while $AlO^{-3/2}$ surface groups are expected to be much less likely at environmental conditions as they involve double deprotonation of the same surface group. The deprotonation schemes 1, 2, and 3 in Figure 2 are, therefore, more likely than scheme 4. In the previous study of Kremleva *et al.* (2016), the relative deprotonation energies corresponding to schemes 1 to 4 were estimated roughly. The lowest and somewhat similar deprotonation energies were estimated for schemes 1 and 2 with differences for various smectite (110) surfaces of <15 kJ mol^{-1} (Kremleva *et al.*, 2016). Scheme 3 was ~40 kJ mol^{-1} higher in energy, while scheme 4 exhibited the greatest deprotonation energy of >100 kJ mol^{-1} (Kremleva *et al.*, 2016).

Both bidentate and monodentate adsorption complexes were investigated. Bidentate adsorption complexes exhibited two An–O_s bonds to the surface O_s centers, while monodentate complexes show only one. The corresponding sites are also called bidentate and monodentate sites. Inspecting various possible adsorption sites, preferential adsorption at deprotonated surface groups was assumed. Then deprotonation scheme 1 results in two adsorption sites (Figure 2): the monodentate AlOH site (m1) and the bidentate AlO_mOH site (b1). In Figure 2, m indicates monodentate and b, bidentate sites. Deprotonation scheme 2 leads to the monodentate Si_lO site and the bidentate AlOH–SiO sites m2 and b2 in Figure 2. In order to differentiate between the two silanol groups present on the (110) surface, subscripts l and u were introduced to label lower and upper monodentate SiO sites, Si_lO and Si_uO, respectively, m2 and m3 in Figure 2. In the case of bidentate groups, the silanol groups involved are obvious, so the subscripts were dropped. Scheme 3 results in monodentate Si_uO and bidentate $SiOO_m$ sites, m3 and b3

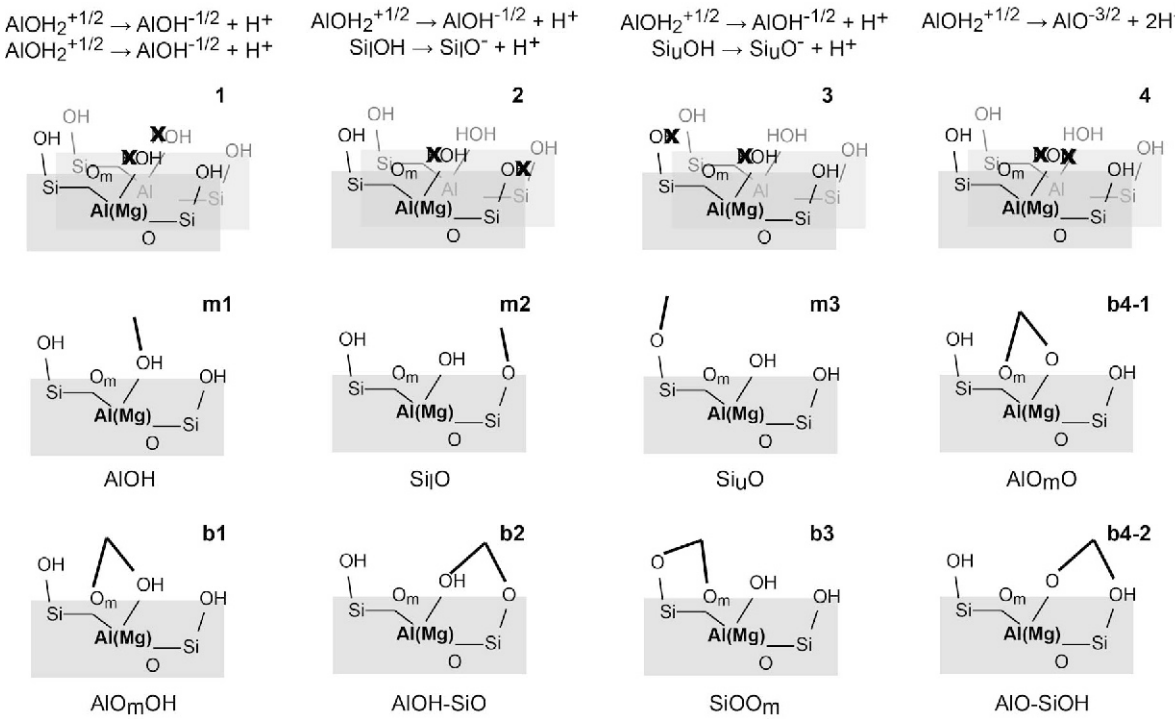

Figure 2. Schematic representation of deprotonated surface groups and adsorption sites studied. The first row shows the surface models (two cells in the *b* direction) with surface groups crossed corresponding to deprotonated groups according to schemes 1–4. (1) Two $AlOH_2$ groups deprotonated; (2) lower SiOH and $AlOH_2$ groups deprotonated; (3) upper SiOH and $AlOH_2$ groups deprotonated; (4) two protons from $AlOH_2$ group removed. The second and third rows show the corresponding adsorption sites. m = monodentate, b = bidentate.

https://doi.org/10.1346/CCMN.2016.0640408 Published online by Cambridge University Press

in Figure 2. For scheme 4, two bidentate sites were considered, AlO_mO and AlO−SiOH, b4-1 and b4-2 in Figure 2. A possible monodentate adsorption complex on the AlO site was also explored. The corresponding starting geometry always converged to bidentate surface complexes at AlO_mO or AlO−SiOH sites.

Solvation is important when studying edge surfaces of clay minerals and adsorption on them (Kremleva *et al.*, 2011). Thus, all surface models of the present study include 19 H_2O molecules per unit cell to account for surface solvation and aquo ligands forming the first solvation shell of actinyls. This number of water molecules was sufficient to create about two layers of water evenly distributed above the surface. The resulting solvated slabs were separated by ~7 Å of vacuum. With this approach, comparison of the total energies of various types of adsorption complexes was possible. Coordination numbers 4 and 5 were tested for NpO_2^+ adsorption complexes. Bidentate uranyl adsorption complexes were taken from the earlier study of Kremleva *et al.* (2016) for comparison. Monodentate uranyl complexes were inspected in the present study for the first time. For uranyl-surface complexes the coordination number 5 was assumed initially as it is the most stable CN for UO_2^{2+} in solution (Denecke *et al.*, 1997; Wahlgren *et al.*, 1999; Vallet *et al.*, 2003) and also most common for adsorption complexes (Catalano and Brown, 2005; Křepelová *et al.*, 2008; Kremleva *et al.*, 2011, 2015).

RESULTS AND DISCUSSION

In the following sections, the adsorbed species determined for U(VI) and Np(V) on unsubstituted and substituted montmorillonite (110) surfaces are discussed first. Then, relative energies of various adsorption complexes and the effect of Mg substitution on the surface are analyzed. Finally, structural parameters of the adsorption complexes are compared with the available experimental data.

Adsorbed species

Unsubstituted surface. The first part of Table 1 lists the resulting species of equilibrated and optimized adsorbed neptunyl and uranyl on unsubstituted sites of the (110) montmorillonite surface. For all the sites inspected, stable adsorption complexes were found. The only exception is NpO_2^+ initially adsorbed on the AlO_mO site (b4-1 in Figure 2) which converged to a complex adsorbed on the AlO_mOH site (b1 in Figure 2). This site was formed by a proton moving from the neighboring SiOH group. Thus, in contrast to uranyl, neptunyl does not form a stable adsorption complex on the AlO_mO site (Table 1).

For the adsorption complexes studied, as in the previous studies on U(VI) (Kremleva *et al.*, 2015, 2016), two types of deviations from the five-coordinated uranyl and neptunyl species constructed initially were observed: reduction of the coordination number to 4 and hydrolysis. A change of the CN from 5 to 4 resulted from the release of one of the aquo ligands of the first coordination shell of the adsorbed actinyl to the solvation layer. In previous studies of U(VI) adsorption on edge surfaces of smectites, mixed AlO(H)-SiO(H) sites were shown to be prone to a reduction of the coordination number of adsorbed uranyl for steric reasons (Kremleva *et al.*, 2015, 2016). For the mont-

Table 1. Adsorbed species, coordination numbers (CN), and relative energies, E_{rel} (kJ mol^{-1}), for bidentate and monodentate adsorption of UO_2^{2+} and NpO_2^+ at various sites on (110) edge surfaces of montmorillonite. For site designations see Figure 2.

Site		Adsorbate	CN	E_{rel}	Adsorbate	CN	E_{rel}
Unsubst.							
AlOH	m1	UO_2OH^+	4	85	NpO_2OH	4	41
AlO_mOH	b1	UO_2OH^+	5	68	NpO_2^+	4/5	86/98
Si_uO	m2	UO_2OH^+	5	23	NpO_2OH	4	36
$SiOO_m$	b2	UO_2OH^+	5	27	NpO_2^+	4/5	80/106
Si_lO	m3	UO_2OH^+	5	13	NpO_2OH	4/5	0/61
AlOH-SiO	b3	UO_2^{2+}	4/5	0/16	NpO_2^+	4/5	15/24
AlO_mO	b4-1	UO_2^{2+}	5	38	–		
AlO-SiOH	b4-2	UO_2^{2+}	4/5	73/73	NpO_2^+	4	127
Subst.							
MgOH	m1	UO_2OH^+	4	104	NpO_2OH	4	22
MgO_mOH	b1	UO_2OH^+	4	78	NpO_2OH/NpO_2^+ *	4/5	71/97
Si_uO	m2	UO_2OH^+	5	31	NpO_2^+	4	52
$SiOO_{Mg}$	b2	UO_2OH^+	5	35	NpO_2^+	4	59
Si_lO	m3	UO_2OH^+	5	21	NpO_2OH	4/5	0/81
MgOH−SiO	b3	UO_2^{2+}	4	0	NpO_2^+	4	26
MgO_mO	b4-1	UO_2^{2+}	4	60	–		
MgO−SiOH	b4-2	UO_2^{2+}	4/5	69/96	NpO_2^+	4	143

* four-coordinated NpO_2OH and five-coordinated NpO_2^+.

https://doi.org/10.1346/CCMN.2016.0640408 Published online by Cambridge University Press

morillonitic model both complexes with CN = 5 and 4 were equilibrated on the AlOH-SiO site, with CN = 5 being 16 kJ mol^{-1} less favorable (Kremleva *et al.*, 2016). For the AlO-SiOH site, the complex with CN = 4 was found to be energetically as stable as that with CN = 5 (Table 1). Among the monodentate uranyl complexes, that at the AlOH site could only be converged with CN = 4. Initially, five-coordinated monodentate complexes on the AlOH site converged to bidentate ones, either at the AlO_mOH or at the AlOH−SiO sites. Uranyl monodentate adsorption complexes on silanol sites remained five-coordinated (Table 1). This can be explained by steric causes. The SiO surface groups are located at the edges of the montmorillonite layer and the $U-O_s$ bond is bent away from the layer, providing space for four aquo ligands in the first coordination shell of uranyl. The AlOH surface group is located in the middle of the mineral layer which implies steric hindrance for four H_2O ligands.

For the adsorption complexes of Np(V), initial structures with both CN = 4 and 5 were constructed. For the complexes adsorbed in monodentate fashion on AlOH and Si_uO, and in bidentate fashion on AlO−SiOH sites, the initially five-coordinated NpO_2^+ converged to CN = 4. For the sites AlOH-SiO, AlO_mOH, $SiOO_m$, and Si_lO, both species with CN = 4 and CN = 5 were equilibrated successfully and optimized. The four-coordinated complexes were calculated to always be more favorable, however (Table 1). The energy differences between CN = 4 and 5 amount to 9, 12, 26, and 61 kJ mol^{-1} for the AlOH-SiO, AlO_mOH, $SiOO_m$, and Si_lO sites, respectively (Table 1). The preference of adsorbed Np(V) for CN = 4 is explained by the lower charge compared to U(VI) together with the bond competition between the aquo ligands and the surface. Aquo ligand extraction energies of five-coordinated U(VI) and Np(V) in the gas phase amounted to 90 and 48 kJ mol^{-1}, respectively. Reduction of the CN from 5 to 4 means that an aquo ligand loses its bond to the actinyl and instead forms two hydrogen bonds, on average, to neighboring water molecules. The energy of forming these two hydrogen bonds was estimated here as 39 kJ mol^{-1} by dissociating $(H_2O)_3$ in the gas phase. These numbers show that the aquo ligand extraction energy of adsorbed Np(V), which should be lower than for the aquo complex due to bond competition with negatively charged surface oxygens, may well fall below the energy of the hydrogen bonds of a water oxygen to its neighbors. This estimate was confirmed in a few cases where the authors were able to stabilize adsorbed Np(V) species with CN = 5, which are all less stable than their four-coordinate congeners.

Another phenomenon observed for actinyl adsorption is the formation of hydrolyzed species on the surface. Hydrolyzed species were calculated for the sites neighboring a deprotonated $AlOH^{-1/2}$ surface group. For UO_2^{2+} adsorbed in bidentate fashion on AlO_mOH and $SiOO_m$ sites and in monodentate fashion on AlOH, Si_uO, and Si_lO sites, one of the aquo ligands in the first coordination shell of uranyl deprotonates. The proton released adsorbs on the neighboring $AlOH^{-1/2}$ surface group which was shown to be a good proton acceptor (Churakov, 2007; Tazi *et al.*, 2012; Liu *et al.*, 2013). As a result, UO_2OH^+ was obtained as an adsorbate (Table 1). The hydrolysis constant of the uranyl aquo complex is ~−4.5 (Grenthe *et al.*, 2004), while the acidity constant of the $AlOH_2^{+1/2}$ surface group is 5.5 (Liu *et al.*, 2013). The uranyl ion is thus inclined to hydrolyze if an $AlOH^{-1/2}$ surface group is nearby.

The hydrolysis of neptunyl on the surface is expected to be less likely as the hydrolysis constant for the aquo complex of Np(V) (reported values vary between −8 and −11.7; Lemire *et al.*, 2001) is estimated to be lower than that for uranyl. Hydrolysis was observed for all monodentate adsorption complexes of Np(V) (Table 1). The proton released was adsorbed on an $AlOH^{-1/2}$ group. In order to test the stability of adsorbed NpO_2OH the equilibrated structures were used to construct an initial geometry with NpO_2^+ as adsorbate by rearranging the protons. As a result of optimization, NpO_2^+ remained as non-hydrolyzed on AlOH and Si_uO sites, being energetically 10 kJ mol^{-1} less stable than the hydrolyzed species. Subsequent equilibration for 1 ps resulted in hydrolyzed species again. This test showed that the non-hydrolyzed and hydrolyzed Np(V) adsorbed species are rather close in terms of energy. On the other hand, this might also be an artefact of the lower cut-off energy used in the AIMD simulation. Hydrolysis of Np(V) on the montmorillonite surface, as found in the present study, should be taken with caution, therefore.

Substituted surface. The lower part of Table 1 shows the adsorbed species on the substituted (110) surface of montmorillonite. In most cases the adsorbed species did not change when an Al^{3+} cation at the surface was substituted by Mg^{2+}. Here only the exceptions are discussed. For uranyl adsorbed on the substituted sites of the (110) montmorillonite surface, CN = 4 became more common than CN = 5 (Table 1). The adsorption complex of UO_2^{2+} on the mixed MgO-SiOH site is preferentially four-coordinated. Adsorption complexes of uranyl on MgO_mO and MgO_mOH sites also converged to CN = 4 during equilibration. This has steric causes, due to rather long O_s-O_s distances of 301 pm between the surface O centers of these sites compared to ~270 pm for the unsubstituted AlO_mO and AlO_mOH sites (Kremleva *et al.*, 2016).

For Np(V) adsorption on the substituted (110) montmorillonite surface, all adsorption complexes were again most stable with CN = 4 (Table 1). Only the two complexes at the MgO_mOH and Si_lO sites could be equilibrated and optimized with CN = 5 (Table 1).

Surface substitution does not affect the formation of adsorbed hydrolyzed species of uranyl. Adsorbed uranyl

https://doi.org/10.1346/CCMN.2016.0640408 Published online by Cambridge University Press

hydrolyzes at all sites where an $AlOH^{-1/2}$ surface group is available to accept a proton (Figure 2) as on the unsubstituted surface (Table 1). While NpO_2OH on the unsubstituted surface is only determined for monodentate adsorption complexes, on the substituted surface a hydrolyzed species appears on MgOH, Si_lO, and MgO_mOH sites (Table 1). In contrast to the unsubstituted surface, on the Si_uO monodentate site NpO_2^+ was equilibrated as an adsorbate. As a test, the hydrolyzed Np(V) adsorption complex on this site was equilibrated. It is less stable, by just 8 kJ mol^{-1}, than the corresponding NpO_2^+ complex, which confirms that hydrolyzed and non-hydrolyzed species of adsorbed Np(V) are close in terms of energy on the potential-energy surface.

Relative energies

In earlier studies on U(VI) adsorption, complex formation energies were estimated as the exchange of two protons from the surface with uranyl (Kremleva *et al*. 2015, 2016). Here, however, only relative energies are discussed as formation energies exhibit significant uncertainties and are referenced to different substrate models for U(VI) and Np(V) and thus are difficult to compare; see section S1 of the supplementary information document deposited in The Clay Minerals Society's website: http://www.clays.org/JOURNAL/JournalDeposits.html.

The most favorable adsorption complex of uranyl on the (110) montmorillonite surface with subsurface substitution was four-coordinated UO_2^{2+} on the AlOH-SiO site (Table 1) (Kremleva *et al.*, 2016). Its 5-coordinated variant was 16 kJ mol^{-1} less favorable. The preference of uranyl adsorption on the AlOH−SiO site was explained previously by the relatively easy deprotonation of the site and a rather large total charge for this site (Kremleva *et al.*, 2016). Monodentate adsorption complexes of UO_2OH^+ on the Si_lO and Si_uO sites are a little less stable and exhibit relative energies of 13 and 23 kJ mol^{-1}, respectively (Table 1). The bidentate complex on the $SiOO_m$ site with an energy difference of 27 kJ mol^{-1} becomes, therefore, the most favorable complex. All the other adsorption complexes exhibit larger relative energies with the least favorable being that at the AlO-SiOH site (Table 1). Thus, for uranyl, the preferred sites with relative energies of <30 kJ mol^{-1} were the AlOH-SiO, Si_lO, Si_uO, and $SiOO_m$ sites. This energy order was preserved for U(VI) adsorption when surface substitution was considered. The most stable sites, in order of increasing relative energy, were MgOH-SiO, Si_lO, Si_uO, and $SiOO_{Mg}$, where the latter three were less stable, by 21, 31, and 35 kJ mol^{-1}, than the most favorable MgOH-SiO site (Table 1). Note that this set of more favorable sites was formed by the surface groups with low deprotonation energies.

In contrast to U(VI), Np(V) preferred monodentate adsorption on the Si_lO site of the (110) montmorillonite surface with subsurface substitution (Table 1). Slightly less favorable was the neptunyl adsorption on the AlOH-SiO site with energy differences of 15 and 24 kJ mol^{-1} for complexes with CN = 4 and 5, respectively (Table 1). All the other complexes exhibited greater relative energies (Table 1). The least favorable site for Np(V) adsorption was the AlO-SiOH site (Table 1). Similar to U(VI), the preferred adsorption sites for Np(V) on the (110) montmorillonite surface were Si_lO and AlOH-SiO (Table 1).

In contrast to U(VI), the energy ordering changed for neptunyl adsorption when the Mg substitution appeared on the surface. The preferred site was still Si_lO (Table 1). The next most stable was the MgOH site, which is only 22 kJ mol^{-1} less favorable than the Si_lO site. Then followed the MgOH-SiO site with the relative energy of 26 kJ mol^{-1} (Table 1). All the other sites exhibited relative energies of >50 kJ mol^{-1}. Thus, the energy order of the most stable adsorption sites for Np(V) on the substituted surface was Si_lO, MgOH, MgOH-SiO, as adsorption at the MgOH site is particularly stable compared to the unsubstituted AlOH site (Figure 3).

The relative energies of all studied adsorption complexes of U(VI) and Np(V) on the (110) surfaces of montmorillonite are illustrated schematically in Figure 3. In order to compare the complexes on slab models with subsurface and surface substitutions, E_{rel} values for the unsubstituted surface were corrected. The neutral montmorillonite (110) surface with a subsurface

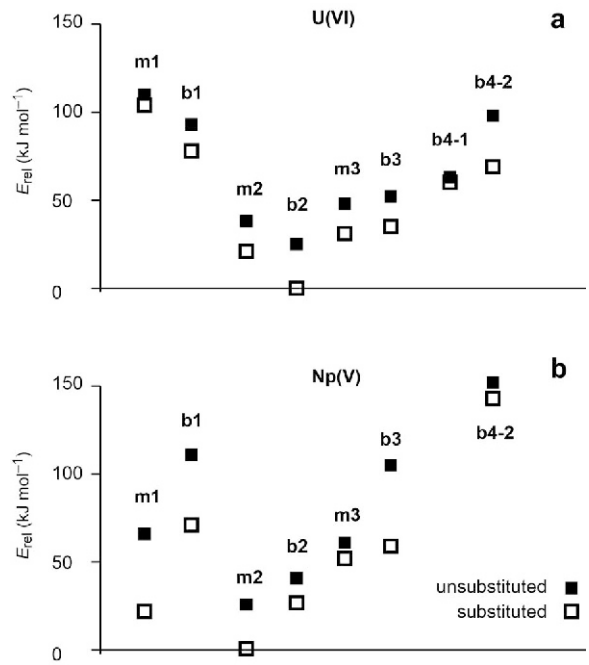

Figure 3. Relative energies of adsorption complexes of: (a) UO_2^{2+} and (b) NpO_2^+ on (110) surfaces of montmorillonite. Filled symbols correspond to species at the unsubstituted surface, empty symbols to species at the substituted surface. For the site designations see Figure 2.

https://doi.org/10.1346/CCMN.2016.0640408 Published online by Cambridge University Press

substitution was 25 kJ mol^{-1} more favorable than the surface with a surface substitution. Thus, 25 kJ mol^{-1} was added to all relative energy values of the adsorption complexes on the unsubstituted (110) montmorillonite surface. This shift is valid only for the neutral surface as a reference. Adsorption on sites on the substituted surface was always more favorable compared to the corresponding unsubstituted surface due to the more negative charge of sites on that surface. U(VI) and Np(V) adsorption on montmorillonite differed by the preference for mono- or bidentate coordination. The pairs of complexes m1 and b1, m2 and b2, and m3 and b3 are monodentate and bidentate adsorption complexes for the same surface deprotonation scheme (Figure 2). U(VI) adsorption tended to prefer bidentate coordination for a given deprotonation scheme, b1 and b2 were lower in energy terms than m1 and m2 (Figure 3a). Adsorption complexes of U(VI) on the silanol sites m3 and b3 are very close in energy terms (Figure 3a). In contrast, for Np(V) adsorption, the monodentate complexes were more favorable than bidentate complexes: m1, m2, and m3 were considerably more favorable than b1, b2, and b3, respectively (Figure 3b).

A surface-complexation model for U(VI) and Np(V) adsorption on montmorillonite proposed strong sites of low density and weak sites of high density (Bradbury and Baeyens, 2005b). As an ideally terminated surface and adsorption sites formed by deprotonation of surface groups of high density were considered here, the present results may be identified with the weak sites of that thermodynamic model. In addition, the calculated relative energies did not show a strong preference for a specific site. Instead, they indicated a set of sites with similar adsorbate binding which should be similar for other edge surfaces. Thus, the proposed strong sites may either be rarely realized deprotonation states or defect sites offering low coordinated oxygens, which have not been considered here.

Structural parameters and comparison with experiment

U(VI) adsorption. Structural parameters of uranyl bidentate adsorption complexes were discussed in detail in previous studies (Kremleva *et al.*, 2015, 2016). Those studies showed that for U(VI) bidentate adsorption on edge surfaces of 2:1 clay minerals, the main structural parameters depended essentially on the surface groups forming the adsorption site and not on the variant of the mineral. The ionic character of uranyl-surface binding was confirmed by a correlation between the charges of the surface O centers and the corresponding $U-O_s$ bond lengths. Here, structural parameters for monodentate adsorption complexes, m1, m2, and m3 in Figure 2, that were not examined previously, are provided and compared with the geometry of corresponding bidentate complexes, b1, b2, and b3 in Figure 2 (Table 2).

Similar to bidentate adsorption complexes, the monodentate complexes exhibited terminal uranyl $U-O_t$ bond lengths of 183–185 pm (Table 2). $U-O_{eq}$ distances for the monodentate adsorption complexes with CN = 5 varied between 241 and 247 pm, while for the 5-coordinated bidentate complexes, $U-O_{eq}$ distances were measured at 242–246 pm (Table 2). $U-O_{eq}$ distances for four-coordinated uranyl adsorption complexes amounted to 230–234 pm for the bidentate complexes and to 233–234 pm for monodentate complexes (Table 2). Thus, for bidentate as well as monodentate adsorption complexes, $U-O_{eq}$ depended essentially on the coordination number of uranyl (Kremleva *et al.*, 2015). $U-O_s$ bond lengths correlated with the charge of the O_s center independent of the coordination mode to the surface. The $U-O_s$ bonds to $AlOH^{-1/2}$ groups measured 232 or 235 pm for mono- and bidentate adsorption complexes (Table 2). $U-O_s$ to the $MgOH^{-2/3}$ surface group were shortened from ~233 pm to 226–228 pm due to substitution for both coordination modes (Table 2). The $U-O_s$ bond lengths to the SiO surface group varied between 214 and 219 pm for most of the adsorption complexes. Longer bonds of 223 pm and 230 pm were calculated for uranyl adsorbed on the Si_lO and $SiOO_{Mg}$ sites (Table 2). Thus, U–O bond lengths of adsorbed uranyl did not depend on the adsorption mode as both bidentate and monodentate adsorption complexes exhibit similar U–O bond lengths (Table 2). The only structural parameter that differed for monodentate complexes compared to bidentate complexes is the shortest U–Al/Mg/Si distance. While for bidentate complexes it can be rather short (305–307 pm for $SiOO_m$ sites, ~350 pm for the Al/MgO_mOH site, and ~360 pm for Al/MgOH-SiO sites), for monodentate complexes these distances were longer. The typical U–Si distance was ~375 pm and U–Al/Mg distances were >400 pm for monodentate coordination (Table 2).

The only structural characteristic that was specific to the adsorption mode (or the corresponding site), therefore, was the U–Al/Mg/Si distance which is not easy to interpret from experimental data. This distance does not represent a chemical bond, it is in the region of multiple scattering, and was not always observed for uranyl adsorption on clay minerals (Sylwester *et al.*, 2000). The monodentate adsorption complexes of U(VI) on silanol sites, m2 and m3, were calculated to be rather close in energy to the most stable adsorption complexes on the Al/MgOH-SiO sites, b2 (Figure 3a). These adsorption complexes might coexist, therefore. A weak hint from EXAFS experiments to the existence of monodentate adsorption complexes may be the coordination numbers of the resolved U–Al/Si distances: they were all <1 (see Table 2). This might mean that not all adsorbed U atoms exhibit Al or Si cation neighbors at a distance of <350 pm. Thus, monodentate adsorption complexes may well contribute to the measured EXAFS spectra.

Np(V) adsorption. The structural parameters of the adsorption complexes of Np(V) on (110) montmorillonite surfaces are shown in Table 3. The more stable

https://doi.org/10.1346/CCMN.2016.0640408 Published online by Cambridge University Press

Table 2. Structural parameters (pm)[a] and relative energies, E_{rel} (kJ mol^{-1}), of U(VI) monodentate and bidentate adsorption complexes for various sites at the unsubstituted and substituted (110) edge surfaces of montmorillonite. For comparison, computational data for the solvated uranyl ion modeled as $UO_2^{2+}(H_2O)_{64}$ with CN = 5 and experimental data with CN in parentheses are given. For site designations see Figure 2.

Site		CN	U−O_t	U−O_s	U−O_s	U−OH	U−O_w	U−O_{eq}	U−Al	U−Si	E_{rel}
$UO_2^{2+}(H_2O)_{64}$		5	181					243			
Unsubst.											
AlOH	m1	4	183	232		216	242	233	404		85
AlO_mOH	b1	5	182	249	235	218	264	246	351		68
Si_uO	m2	5	185	214		228	254	241		376	23
$SiOO_m$	b2	5	185	218	261	232	253	243		307	27
Si_lO	m3	5	184	219		219	265	247		375	13
AlOH-SiO	b3	4	183	232	215		240	232	396	356	0
		5	183	232	216		256	243	404	360	16
Subst.									U−Mg		
MgOH	m1	4	183	228		217	246	234	425		104
MgO_mOH	b1	4	182	233	227	231	246	234	354		78
Si_uO	m2	5	185	217		229	254	242		377	31
$SiOO_{Mg}$	b2	5	183	230	243	232	254	242		305	35
Si_lO	m3	5	183	223		217	265	247		378	21
MgOH-SiO	b3	4	183	226	219		238	230	395	362	0
Exp.	Ref.	pH	U−O_t		U−O_s		U−O_w	U−O_{eq}	U−Al/Si/Fe		
UO_2^{2+}	*b*	4	176(2.0)					241(5.0)			
Mont	*c*	6.4	178(2.0)					236(6.2)	343(0.6)		
	d	6.6	179(2.3)		229(2.1)		247(2.1)	238(4.2)	331(0.6)		
	e	7	180(2.0)		232(2.8)		248(2.1)	234(5.0)	342(0.2)		
	f	8	180(2.0)		230(3.1)		248(2.9)	239(6.0)	328(0.9)	309(0.9)	

[a] Average terminal uranyl bond length U−O_t, bond lengths U−O_s to surface oxygen centers in the order of the sites label, U−OH bond length to OH ligands, average bond length U−O_w to aquo ligands, average equatorial U−O bond lengths U−O_{eq}, U−Al/Mg and U−Si distances to the nearest surface Al/Mg and Si centers.
[b] Allen *et al.* (1997); [c] Hennig *et al.* (2002); [d] Schlegel and Descostes (2009); [e] Catalano and Brown (2005), W5N sample. [f] Marques Fernandes *et al.* (2012).

species were chosen from those equilibrated and optimized for the same site. Only adsorption complexes with CN = 4 are shown in Table 3, therefore. The only exception is the AlOH-SiO site where both four- and five-coordinated isomers are given in Table 3, as they differ by only 9 kJ mol^{-1} in energy and both exhibit relatively low E_{rel} values. Representative structures of more stable complexes are shown in Figure 4.

To the best of the authors' knowledge, no EXAFS data exist for Np(V) adsorbed on montmorillonite or any other 2:1 clay mineral. Experiments on gibbsite and kaolinite have been carried out, however (Amayri *et al.*, 2008; Gückel *et al.*, 2013). Gibbsite is one of the mineral forms of Al hydroxide and offers only aluminol groups for adsorption. Kaolinite is a 1:1 aluminosilicate which shows two types of basal surfaces: an Al octahedral hydroxylated surface, similar to gibbsite, and a Si tetrahedral surface similar to the basal surfaces of montmorillonite. Comparison of EXAFS data for U(VI) adsorption showed that structural data for montmorillonite (Catalano and Brown, 2005; Hennig *et al.*, 2002; Marques Fernandes *et al.*, 2012; Schlegel and Descostes, 2009) compare well with data for kaolinite (Křepelová *et al.*, 2008) and only slightly worse for gibbsite (Arnold *et al.*, 2006); see section S2 of the supplementary information file deposited at http://www.clays.org/JOURNAL/JournalDeposits.html. As comparable differences are expected in the structures of adsorption complexes of Np(V), the structures of adsorbed Np(V) on montmorillonite may be compared to available EXAFS data of Np(V) adsorption on kaolinite and gibbsite (Amayri *et al.*, 2008; Gückel *et al.*, 2013). The EXAFS measurements of Np(V) adsorption on gibbsite resolved a Np−C distance of 292 pm with CN = 0.8 (Gückel *et al.*, 2013) which points to the formation of carbonato complexes at the surface, which were not modeled in the present study. The EXAFS data for kaolinite are preferred (Amayri *et al.*, 2008) for comparison, therefore. The experiment on Np(V) adsorption on kaolinite resolved only Np−O_t and a single Np−O_{eq} distance (Amayri *et al.*, 2008). In contrast to U(VI) adsorption on montmorillonite and also kaolinite (Křepelová *et al.*, 2008; Schlegel and Descostes, 2009; Marques Fernandes *et al.*, 2012), no splitting of the Np−O bond lengths in the equatorial shell in two groups was observed experimentally.

https://doi.org/10.1346/CCMN.2016.0640408 Published online by Cambridge University Press

Table 3. Structural parameters (pm)[a] and relative energies, E_{rel} (kJ mol^{-1}), of Np(V) monodentate and bidentate adsorption complexes for various sites at the unsubstituted and substituted (110) edge surfaces of montmorillonite. For comparison, computational data for the solvated neptunyl ion modeled as $NpO_2^+(H_2O)_{64}$ with CN = 4 and 5 and experimental data with CN in parentheses are given. For site designations see Figure 2.

Site		CN	Np−O_t	Np−O_s	Np−O_s	Np−OH	Np−O_w	Np−O_{eq}	Np−Al	Np−Si	E_{rel}
$NpO_2^+(H_2O)_{64}$		4	185					244			
$NpO_2^+(H_2O)_{64}$		5	185					253			
Unsubst.											
AlOH	m1	4	188	232		231	247	239	401		41
AlO_mOH	b1	4	184	246	238		242	242	347	351	86
Si_uO	m2	4	187	220		235	247	237		377	36
$SiOO_m$	b2	4	187	232	258		241	243	420	306	80
Si_lO	m3	4	186	230		236	246	240		366	0
AlOH−SiO	b3	4	184	240	231		246	241	392	359	15
		5	185	234	231		265	252	395	362	24
AlO−SiOH	b4-2	4	188	203	252		256	242	368	385	127
Subst.									Np−Mg		
MgOH	m1	4	189	228		230	249	239			22
MgO_mOH	b1	4	187	239	233	235	237	236	340	373	71
Si_uO	m2	4	186	218			248	241		379	52
$SiOO_{Mg}$	b2	4	185	232	245		250	244		300	59
Si_lO	m3	4	186	233		221	256	242		366	0
MgOH−SiO	b3	4	185	229	232		247	239		366	26
MgO−SiOH	b4-2	4	190	197	250		251	237	370	385	143
Exp.	Ref.	pH	Np−O_t					Np−O_{eq}			
NpO_2^+	*b*		182(2)					249(3.6)			
Kaolinite	*c*	8	185(2)					245(4)			
	c	9	186(2)					250(4)			
	c	10	187(2)					247(4)			

[a]Average terminal neptunyl bond length Np−O_t, bond lengths Np−O_s to surface oxygen centers in the order of the sites label, Np−OH bond length to OH ligands, average bond length Np−O_w to aquo ligands, average equatorial Np−O bond lengths Np−O_{eq}, and Np−Al/Mg and Np−Si distances to the nearest surface Al/Mg and Si centers.
[b] Reich *et al.* (2000); [c] Amayri *et al.* (2008).

Because of the low signal-to-noise ratio, the Np-Al/Si shell was not modeled (Amayri *et al.*, 2008). In order to estimate the effect of adsorption on the main structural parameters of Np(V), the EXAFS data for the solvated Np(V) ion was also provided (Reich *et al.*, 2000). Various EXAFS studies on solvated Np(V), with reported CN from 4 to 6, with Np−O_t bond lengths of 180 to 185 pm, and Np−O_{eq} distances of between 244 and 252 pm (Combes *et al.*, 1992; Allen *et al.*, 1997; Reich *et al.*, 2000; Antonio *et al.*, 2001; Ikeda-Ohno *et al.*, 2008). For comparison, data from an experiment carried out by the same group which measured EXAFS for adsorbed Np(V) on kaolinite was chosen (Reich *et al.*, 2000). The main effect of Np(V) adsorption on kaolinite on the structural parameters of neptunyl as measured by EXAFS was the elongation of the Np−O_t bond by 3−5 pm (185−187 pm *vs*. 182 pm for the solvated NpO_2^+ ion) and a tendency toward shorter Np−O_{eq} (245−250 pm *vs*. 249 pm) (Amayri *et al.*, 2008). The coordination number of neptunyl was fixed at 4 in fitting these data (Amayri *et al.*, 2008).

The calculated Np−O_t bonds of the adsorption complexes varied from 184 to 190 pm and were, on average, longer than Np−O_t in the aquo complexes, 185 pm (Table 3). Np−O_t tended to be shorter by ~2 pm for bidentate adsorption, 184−187 pm, than for monodentate complexes, 186−189 pm, when corresponding sites are compared (Table 3). The calculated Np−O_t bonds compare well with the experiment which yielded 185−187 pm (Amayri *et al.*, 2008). For the b4-2 sites, Np−O_t values were longest, 188 and 190 pm, due to rather short (and therefore strong) bonds Np−O_s to $AlO^{-3/2}$ and $MgO^{-5/3}$ groups, 197 and 203 pm, respectively (Table 3). Np−O_s bond lengths in the monodentate complexes were shorter than Np−O_s to the same surface O_s center in the corresponding bidentate adsorption complexes due to bond competition (Table 3). This is in line with the lower relative energies calculated for monodentate adsorption of Np(V) (Table 3). The An−O_s bond lengths cannot be used as an indication of the energetic preference of mono- or bidentate coordination, however. For U(VI) adsorption, similar trends were observed in general, although U−O_t of monodentate complexes are, on average, 1 pm greater than U−O_t of bidentate complexes (Table 2). On the other hand, U−O_s bonds in some monodentate U(VI)

https://doi.org/10.1346/CCMN.2016.0640408 Published online by Cambridge University Press

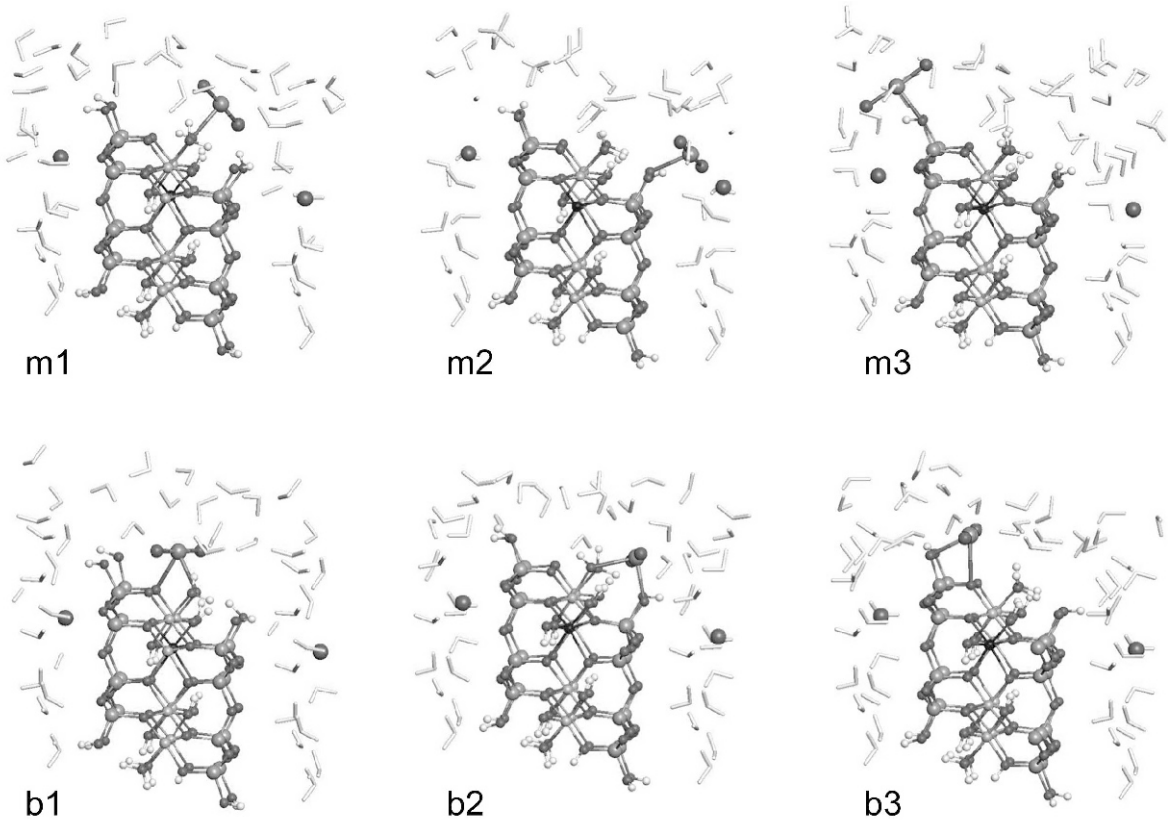

Figure 4. Representative structures of more stable adsorption complexes of Np(V) on the (110) edge surface of montmorillonite with inner substitution. For simplicity, water molecules are shown as light gray sticks.

complexes were longer than the corresponding U−O_s in bidentate complexes (Table 2) and from an energetic point of view, bidentate adsorption complexes were always more favorable.

The average equatorial Np−O_{eq} distances for four-coordinated Np(V) adsorption complexes varied from 237 to 244 pm. They tended to be shorter than Np−O_{eq} = 244 pm as calculated for the solvated Np(V) ion with CN = 4 (Table 3). Five-coordinated adsorption complexes showed Np−O_{eq} between 250 and 253 pm (Table 3, section S3 of the supplementary information document deposited in The Clay Minerals Society's website: http://www.clays.org/JOURNAL/JournalDeposits.html) which compares well with Np−O_{eq} of the solvated penta-aquo ion of 253 pm (Table 3). Thus, as for U(VI), Np−O_{eq} is essentially determined by the CN of NpO_2^+, independent of the adsorption mode or adsorption site (Kremleva *et al.*, 2015).

Np−O_s bond lengths to $AlOH^{-1/2}$ surface groups at the unsubstituted surface varied between 232 and 240 pm, m1, b1, b2 sites (Table 3). Np−O_s distances to the corresponding substituted $MgOH^{-2/3}$ surface group were calculated as being shorter, 228−233 pm, in accordance with the increasing charge of the O_s center. Np−O_s bonds to SiO surface groups varied between 218 and 233 pm in length (Table 3). The ranges of these three types of Np−O_s bond lengths overlap. Even though, on average, they decrease with the increasing charge of O_s, their differences are less pronounced than for uranyl where they showed separate ranges: U−O_s to $AlOH^{-1/2}$ groups measured 232−235 pm, to $MgOH^{-2/3}$ 226−228 pm, and to SiO 214−223 pm (Table 2). In some EXAFS studies on U(VI) adsorption on montmorillonite, two equatorial U−O shells were resolved, with U−O = ~230 pm and ~250 pm. In previous work (Kremleva *et al.*, 2015), the shorter distance was assigned to U−O bonds to the surface groups SiO and $AlOH^{-1/2}$ or to U−OH bonds, while the longer distance was assigned to U−O bonds to O_m centers, SiOH groups, or aquo ligands. The former group of shorter U−O bonds contains bond lengths between 214 and 232 pm. The groups of longer U−O bonds includes U−O_w distances of complexes with CN = 4 (238−246 pm), and 5 (253−265 pm), and U−O_s bonds to the O_m centers of 249−261 pm (Table 2). The two groups of U−O distances (shorter and longer) are rather distinct, especially for the complexes with CN = 5. Although equatorial Np−O distances followed the same trend as for U−O, they are longer for the O centers with

https://doi.org/10.1346/CCMN.2016.0640408 Published online by Cambridge University Press

smaller charges. In contrast to U−O, Np−O bonds did not separate into distinct groups. The EXAFS experiments are not expected to be able to differentiate between various types of equatorial Np−O bonds, therefore, as had been done tentatively for U(VI) (Catalano and Brown, 2005; Schlegel and Descostes, 2009; Marques Fernandes *et al.*, 2012). For Np(V) adsorption on kaolinite, no splitting of the equatorial Np−O shell was found (Amayri *et al.*, 2008).

To summarize, reasonable agreement was found for the geometry of more favorable adsorption complexes of Np(V) with available EXAFS data. Note that EXAFS measures all the species present on a surface and averages their structural parameters. Invoking a surface complexation model (Bradbury and Baeyens, 2005b), due to their much higher site density, the main contribution to EXAFS spectra should stem from adsorption on weak sites, which is in line with a tentative interpretation of the present energy results.

CONCLUSIONS

For the first time, Np(V) adsorption on a clay mineral surface, using the example of the (110) edge surface of montmorillonite, was investigated computationally. Using the quantum chemical density functional approach and a recently developed low-temperature equilibration procedure (Kremleva *et al.*, 2016) for the determination of reliable energies, various monodentate and bidentate Np(V) adsorption complexes were studied and the results were compared to U(VI) adsorption. Both four- and five-coordinated adsorption complexes of NpO_2^+ were modeled.

As for uranyl, four- and five-coordinated NpO_2^+ adsorption complexes were observed. While adsorbed uranyl changed its coordination number for some sites from 5 to 4 mainly for steric reasons, the neptunyl adsorbed always preferred CN = 4. As in the case of U(VI), non-hydrolyzed and hydrolyzed species of Np(V) at the surface were observed. The hydrolyzed uranyl species UO_2OH^+ always formed when an $AlOH^{-1/2}$ surface group was present. The hydrolyzed species NpO_2OH was not always formed when a deprotonated $AlOH^{-1/2}$ surface group was nearby and was mainly observed for monodentate adsorption. The hydrolyzed species of Np(V) on the surface seems, thus, to be less stable than hydrolyzed uranyl, in agreement with the lower hydrolysis constant of the Np(V) aquo ion compared to U(VI). Comparing relative energies, uranyl was shown to prefer bidentate adsorption with the AlOH-SiO site being the most stable at the (110) surface. In contrast, neptunyl adsorbed preferentially as a monodentate complex; the most favorable adsorption site was the Si_lO site. For both actinyls, mono- and bidentate adsorption complexes might coexist, however, as energy differences between more favorable adsorption complexes were small.

Both monodentate and bidentate adsorption complexes of the same actinyl exhibited rather similar structural parameters. Calculated changes in the bond lengths Np−O_t and Np−O_{eq} due to adsorption were compared to experimental results for kaolinite, because no data were available for montmorillonite. Good agreement was found for these geometry parameters. Mono- and bidentate adsorption complexes of neptunyl may be distinguished experimentally by their Np−Al/Si/Mg distances, which were not resolved in the available experiment for kaolinite, unfortunately.

ACKNOWLEDGMENTS

The present study was supported by the German Bundesministerium für Wirtschaft und Energie (grant no. 02E11001). The authors acknowledge a generous grant of computing resources by the Gauss Centre for Supercomputing (www.gauss-centre.eu), provided on the SuperMUC platform of the Leibniz Supercomputing Centre Garching, Germany (www.lrz.de).

SUPPLEMENTARY INFORMATION

A ‘Supplementary Information’ document which includes: discussion on formation energies and their uncertainties; EXAFS data for U(VI) aquo ion and adsorption complexes on various minerals; and a table with the structural data of Np(V) adsorption complexes, is available at http://www.clays.org/JOURNAL/JournalDeposits.html.

REFERENCES

Allen, P.G., Bucher, J.J., Shuh, D.K., Edelstein, N.M., and Reich, T. (1997) Investigation of aquo and chloro complexes of UO_2^{2+}, NpO_2^+, Np^{4+}, and Pu^{3+} by X-ray absorption fine structure spectroscopy. *Inorganic Chemistry*, **36**, 4676−4683.

Amayri, S., Banik, N.L., Breckheimer, M., Buda, R.A., Burger, S., Drebert, J., Jermolajev, A., Kratz, J.V., Kuczewski, B., Kutscher, D., Reich, T.Y., Reich, T., and Trautmann, N. (2008) Interaction of neptunium and plutonium with humic substances and kaolinite. Pp. 141−216 in: *Migration of Actinides in the System Clay, Humic Substances, Aquifer* (C.M. Marquardt, editor). FZKA 7407, Forschungszentrum Karlsruhe, Karlsruhe, Germany.

Amayri, S., Jermolajev, A., and Reich, T. (2011) Neptunium(V) sorption on kaolinite. *Radiochimica Acta*, **99**, 349−357.

Antonio, M.R., Soderholm, L., Williams, C.W., Blaudeau, J.P., and Bursten, B.E. (2001) Neptunium redox speciation. *Radiochimica Acta*, **89**, 17−25.

Arai, Y., Moran, P.B., Honeyman, B.D., and Davis, J.A. (2007) In situ spectroscopic evidence for neptunium(V)-carbonate inner-sphere and outer-sphere ternary surface complexes on hematite surfaces. *Environmental Science & Technology*, **41**, 3940−3944.

Arnold, T., Scheinost, A.C., Baumann, N., and Brendler, V. (2006) Surface speciation of uranyl (VI) on gibbsite: A combined spectroscopic approach. P. 53 in: *Annual Report* (G. Bernhard, editor). Institute of Radiochemistry, Dresden-Rossendorf, Germany.

Benedicto, A., Begg, J.D., Zhao, P., Kersting, A.B., Missana, T., and Zavarin, M. (2014). Effect of major cation water

https://doi.org/10.1346/CCMN.2016.0640408 Published online by Cambridge University Press

composition on the ion exchange of Np(V) on montmorillonite: NpO_2^+–Na^+–K^+–Ca^{2+}–Mg^{2+} selectivity coefficients. *Applied Geochemistry*, **47**, 177–185.

Bidoglio, G., Tanet, G., and Chatt, A. (1985) Studies on neptunium (V) carbonate complexes under geologic repository conditions. *Radiochimica Acta*, **38**, 21–26.

Blöchl, P.E. (1994) Projector augmented wave method. *Physical Review B*, **50**, 17953–17979.

Bradbury, M.H. and Baeyens, B. (2005a) Experimental measurements and modeling of sorption competition on montmorillonite. *Geochimica et Cosmochimica Acta*, **69**, 4187–4197.

Bradbury, M.H. and Baeyens, B. (2005b) Modelling the sorption of Mn(II), Co(II), Ni(II), Zn(II), Cd(II), Eu(III), Am(III), Sn(IV), Th(IV), Np(V) and U(VI) on montmorillonite: Linear free energy relationships and estimates of surface binding constants for some selected heavy metals and actinides. *Geochimica et Cosmochimica Acta*, **69**, 875–892.

Butler, D. (2010) France digs deep for nuclear waste. *Nature*, **466**, 804–805.

Catalano, J.G. and Brown, G.E. (2005) Uranyl adsorption onto montmorillonite: Evaluation of binding sites and carbonate complexation. *Geochimica et Cosmochimica Acta*, **69**, 2995–3005.

Chisholm-Brause, C., Conradson, S.D., Buscher, C.T., Eller, P.G., and Morris, D.E. (1994) Speciation of uranyl sorbed at multiple binding-sites on montmorillonite. *Geochimica et Cosmochimica Acta*, **58**, 3625–3631.

Churakov, S.V. (2007) Structure and dynamics of the water films confined between edges of pyrophyllite: A first principle study. *Geochimica et Cosmochimica Acta*, **71**, 1130–1144.

Combes, J.M., Chisholm-Brause, C.J., Brown, G.E., Parks, G.A., Conradson, S.D., Eller, P.G., Triay, I.R., Hobart, D.E., and Meijer, A. (1992) EXAFS spectroscopic study of neptunium(V) sorption at the alpha-FeOOH water interface. *Environmental Science & Technology*, **26**, 376–382.

Cotton, S. (2006) *Lanthanide and Actinide Chemistry*. Wiley, Chichester, UK.

Del Nero, M., Assada, A., Madé, B., Barillon, R., and Duplâtre, G. (2004) Surface charges and Np(V) sorption on amorphous Al and Fe silicates. *Chemical Geology*, **211**, 15–45.

Den Auwer, C., Drot, R., Simoni, E., Conradson, S.D., Gailhanou, M., and de Leon, J.M. (2003) Grazing incidence XAFS spectroscopy of uranyl sorbed onto TiO_2 rutile surfaces. *New Journal of Chemistry*, **27**, 648–655.

Denecke, M.A., Reich, T., Pompe, S., Bubner, M., Heise, K.H., Nitsche, H., Allen, P.G., Bucher, J.J., Edelstein, N.M., and Shuh, D.K. (1997) Differentiating between monodentate and bidentate carboxylate ligands coordinated to uranyl ions using EXAFS. *Journal de Physique IV*, **7**, 637–638.

Dent, A.J., Ramsay, J.D.F., and Swanton, S.W. (1992) An EXAFS study of uranyl-ion in solution and sorbed onto silica and montmorillonite clay colloids. *Journal of Colloid and Interface Science*, **150**, 45–60.

Fröhlich, D.R. (2015). Sorption of neptunium on clays and clay minerals – a review. *Clays and Clay Minerals*, **63**, 262–276.

Geckeis, H., Lützenkirchen, J., Polly, R., Rabung, T., and Schmidt, M. (2013) Mineral–water interface reactions of actinides. *Chemical Reviews*, **113**, 1016–1062.

Greathouse, J.A. and Cygan, R.T. (2005) Molecular dynamics simulation of uranyl(VI) adsorption equilibria onto an external montmorillonite surface. *Physical Chemistry Chemical Physics*, **7**, 3580–3586.

Greathouse, J.A. and Cygan, R.T. (2006) Water structure and aqueous uranyl(VI) adsorption equilibria onto external surfaces of beidellite, montmorillonite, and pyrophyllite: Results from molecular simulations. *Environmental Science & Technology*, **40**, 3865–3871.

Grenthe, I., Fuger, J., Konings, R., Lemire, R., Muller, A., Nguyen-Trung, C., and Wanner, H. (2004) *Chemical Thermodynamics of Uranium*. OECD Publications, Paris.

Gückel, K., Rossberg, A., Müller, K., Brendler, V., Bernhard, G., and Foerstendorf, H. (2013) Spectroscopic identification of binary and ternary surface complexes of Np(V) on gibbsite. *Environmental Science & Technology*, **47**, 14418–14425.

Hennig, C., Reich, T., Dähn, R., and Scheidegger, A.M. (2002) Structure of uranium sorption complexes at montmorillonite edge sites. *Radiochimica Acta*, **90**, 653–657.

Ikeda-Ohno, A., Hennig, C., Rossberg, A., Funke, H., Scheinost, A.C., Bernhard, G., and Yaita, T. (2008) Electrochemical and complexation behavior of neptunium in aqueous perchlorate and nitrate solutions. *Inorganic Chemistry*, **47**, 8294–8305.

Kosmulski, M. (2012) IEP as a parameter characterizing the pH-dependent surface charging of materials other than metal oxides. *Advances in Colloid and Interface Science*, **171–172**, 77–86.

Kowal-Fouchard, A., Drot, R., Simoni, E., and Ehrhardt, J.J. (2004) Use of spectroscopic techniques for uranium (VI)/montmorillonite interaction modeling. *Environmental Science & Technology*, **38**, 1399–1407.

Kremleva, A., Krüger, S., and Rösch, N. (2008) Density functional model studies of uranyl adsorption on (001) surfaces of kaolinite. *Langmuir*, **24**, 9515–9524.

Kremleva, A., Krüger, S., and Rösch, N. (2011) Uranyl adsorption at (010) edge surfaces of kaolinite: A density functional study. *Geochimica et Cosmochimica Acta*, **75**, 706–718.

Kremleva, A., Krüger, S., and Rösch, N. (2015) Uranyl adsorption at solvated edge surfaces of 2:1 smectites. A density functional study. *Physical Chemistry Chemical Physics*, **17**, 13757–13768.

Kremleva, A., Krüger, S., and Rösch, N. (2016) Toward a reliable energetics of adsorption at solvated mineral surfaces: A computational study of uranyl (VI) on 2:1 clay minerals. *Journal of Physical Chemistry C*, **120**, 324–335.

Křepelová, A., Reich, T., Sachs, S., Drebert, J., and Bernhard, G. (2008) Structural characterization of U(VI) surface complexes on kaolinite in the presence of humic acid using EXAFS spectroscopy. *Journal of Colloid and Interface Science*, **319**, 40–47.

Kresse, G. and Furthmüller, J. (1996a) Efficiency of ab-initio total energy calculations for metals and semiconductors using a plane-wave basis set. *Computational Materials Science*, **6**, 15–50.

Kresse, G. and Furthmüller, J. (1996b) Efficient iterative schemes for ab initio total-energy calculations using a plane-wave basis set. *Physical Review B*, **54**, 11169–11186.

Kresse, G. and Hafner, J. (1993a) Ab initio molecular dynamics for liquid metals. *Physical Review B*, **47**, 558–561.

Kresse, G. and Hafner, J. (1993b) Ab initio molecular dynamics for open shell transition metals. *Physical Review B*, **48**, 13115–13118.

Kresse, G. and Hafner, J. (1994) Ab initio molecular dynamics simulation of the liquid metal amorphous semiconductor transition in germanium. *Physical Review B*, **49**, 14251–14269.

Kresse, G. and Joubert, D. (1999) From ultrasoft pseudopotentials to the projector augmented-wave method. *Physical Review B*, **59**, 1758–1775.

Lectez, S., Roques, J., Salanne, M., and Simoni, E. (2012) Car-Parrinello molecular dynamics study of the uranyl behaviour

at the gibbsite/water interface. *The Journal of Chemical Physics*, **137**, 154705.

Lemire, R., Fuger, J., Nitsche, H., Potter, P., Rand, M., Rydberg, J., Spahiu, K., Sullivan, J., Ullman, W., Vitorge, P., and Wanner, H. (2001) *Chemical Thermodynamics of Neptunium and Plutonium*. Elsevier, Amsterdam.

Liu, X., Lu, X., Sprik, M., Cheng, J., Meijer, E. J., and Wang, R. (2013) Acidity of edge surface sites of montmorillonite and kaolinite. *Geochimica et Cosmochimica Acta*, **117**, 180–190.

Liu, X.D., Cheng, J., Sprik, M., Lu, X.C., and Wang, R.C. (2014) Surface acidity of 2:1-type dioctahedral clay minerals from first principles molecular dynamics simulations. *Geochimica et Cosmochimica Acta*, **140**, 410–417.

Lo, C. and Trout, B.L. (2004). Density-functional theory characterization of acid sites in chabazite. *Journal of Catalysis*, **227**, 77–89.

MacDonald, A.H., Pickett, W.E., and Koelling, D.D. (1980) A linearized relativistic augmented-plane-wave method utilizing approximate pure spin basis functions. *Journal of Physics C – Solid State Physics*, **13**, 2675–2683.

MacDonald, A.H. and Vosko, S.H. (1979) Relativistic density functional formalism. *Journal of Physics C – Solid State Physics*, **12**, 2977–2990.

Marques Fernandes, M., Baeyens, B., Dähn, R., Scheinost, A.C., and Bradbury, M.H. (2012) U(VI) sorption on montmorillonite in the absence and presence of carbonate: A macroscopic and microscopic study. *Geochimica et Cosmochimica Acta*, **93**, 262–277.

Morris, D.E., Chisholm-Brause, C.J., Barr, M.E., Conradson, S.D., and Eller, P.G. (1994) Optical spectroscopic studies of the sorption of UO_2^{2+} species on a reference smectite. *Geochimica et Cosmochimica Acta*, **58**, 3613–3623.

Müller, K., Foerstendorf, H., Brendler, V., and Bernhard, G. (2009) Sorption of Np(V) onto TiO_2, SiO_2, and ZnO: An in situ ATR FT-IR spectroscopic study. *Environmental Science & Technology*, **43**, 7665–7670.

Müller, K., Foerstendorf, H., Meusel, T., Brendler, V., Lefevre, G., Comarmond, M.J., and Payne, T.E. (2012) Sorption of U(VI) at the TiO_2-water interface: An in situ vibrational spectroscopic study. *Geochimica et Cosmochimica Acta*, **76**, 191–205.

Niitsu, Y., Sato, S., Ohashi, H., Sakamoto, Y., Nagao, S., Ohnuki, T., and Muraoka, S. (1997) Effects of humic acid on the sorption of neptunium(V) on kaolinite. *Journal of Nuclear Materials*, **248**, 328–332.

Pauling, L. (1929) The principles determining the structure of complex ionic crystals. *Journal of the American Chemical Society*, **51**, 1010–1026.

Perdew, J.P. and Wang, Y. (1992) Accurate and simple analytic representation of the electron gas correlation energy. *Physical Review B*, **45**, 13244–13249.

Reich, T., Bernhard, G., Geipel, G., Funke, H., Hennig, C., Rossberg, A., Matz, W., Schell, N., and Nitsche, H. (2000) The Rossendorf beam line ROBL – a dedicated experimental station for XAFS measurements of actinides and other radionuclides. *Radiochimica Acta*, **88**, 633–637.

Reich, T., Reich, T.Y., Amayri, S., Drebert, J., Banik, N.L., Buda, R.A., Kratz, J.V., and Trautmann, N. (2007) Application of XAFS spectroscopy to actinide environmental science. *AIP Conference Proceedings*, **882**, 179–183.

Schlegel, M.L. and Descostes, M. (2009) Uranium uptake by hectorite and montmorillonite: A solution chemistry and polarized EXAFS study. *Environmental Science & Technology*, **43**, 8593–8598.

Schmeide, K. and Bernhard, G. (2010) Sorption of Np(V) and Np(IV) onto kaolinite: Effects of pH, ionic strength, carbonate and humic acid. *Applied Geochemistry*, **25**, 1238–1247.

Sylwester, E.R., Hudson, E.A., and Allen, P.G. (2000) The structure of uranium (VI) sorption complexes on silica, alumina, and montmorillonite. *Geochimica et Cosmochimica Acta*, **64**, 2431–2438.

Tazi, S., Rotenberg, B., Salanne, M., Sprik, M., and Sulpizi, M. (2012) Absolute acidity of clay edge sites from ab-initio simulations. *Geochimica et Cosmochimica Acta*, **94**, 1–11.

Tettenhorst, R. and Roberson, H.E. (1973) X-ray-diffraction aspects of montmorillonites. *American Mineralogist*, **58**, 73–80.

Tochiyama, O., Yamazaki, H., and Mikami, T. (1996) Sorption of neptunium(V) on various aluminum oxides and hydrous aluminum oxides. *Radiochimica Acta*, **73**, 191–198.

Turner, D.R., Pabalan, R.T., and Bertetti, F.P. (1998) Neptunium(V) sorption on montmorillonite: An experimental and surface complexation modeling study. *Clays and Clay Minerals*, **46**, 256–269.

Vallet, V., Moll, H., Wahlgren, U., Szabo, Z., and Grenthe, I. (2003) Structure and bonding in solution of dioxouranium(VI) oxalate complexes: Isomers and intramolecular ligand exchange. *Inorganic Chemistry*, **42**, 1982–1993.

Wahlgren, U., Moll, H., Grenthe, I., Schimmelpfennig, B., Maron, L., Vallet, V., and Gropen, O. (1999) Structure of uranium(VI) in strong alkaline solutions. A combined theoretical and experimental investigation. *Journal of Physical Chemistry A*, **103**, 8257–8264.

Zavarin, M., Powell, B.A., Bourbin, M., Zhao, P., and Kersting, A.B. (2012) Np(V) and Pu(V) ion exchange and surface-mediated reduction mechanisms on montmorillonite. *Environmental Science & Technology*, **46**, 2692–2698.

(*Received 28 November 2015; revised 1 July 2016; AE: Xiandong Liu; Ms. 1074*)